Available online at www.sciencedirect.com
ScienceDirect
Journal of Computational Physics 220 (2007) 772–790
JOURNAL OF COMPUTATIONAL PHYSICS
www.elsevier.com/locate/jcp

On the use of the resting potential and level set methods for identifying ischemic heart disease: An inverse problem

Bjørn Fredrik Nielsen *, Marius Lysaker, Aslak Tveito

Simula Research Laboratory, Scientific Computing, Martin Linges vei 17, 1325 Lysaker, Norway

Received 11 November 2005; received in revised form 22 May 2006; accepted 23 May 2006
Available online 17 July 2006

Abstract

The electrical activity in the heart is modeled by a complex, nonlinear, fully coupled system of differential equations. Several scientists have studied how this model, referred to as the bidomain model, can be modified to incorporate the effect of heart infarctions on simulated ECG (electrocardiogram) recordings.

We are concerned with the associated inverse problem; how can we use ECG recordings and mathematical models to identify the position, size and shape of heart infarctions? Due to the extreme CPU efforts needed to solve the bidomain equations, this model, in its full complexity, is not well-suited for this kind of problems. In this paper we show how biological knowledge about the resting potential in the heart and level set techniques can be combined to derive a suitable stationary model, expressed in terms of an elliptic PDE, for such applications. This approach leads to a nonlinear ill-posed minimization problem, which we propose to regularize and solve with a simple iterative scheme.

Finally, our theoretical findings are illuminated through a series of computer simulations for an experimental setup involving a realistic heart in torso geometry. More specifically, experiments with synthetic ECG recordings, produced by solving the bidomain model, indicate that our method manages to identify the physical characteristics of the ischemic region(s) in the heart. Furthermore, the ill-posed nature of this inverse problem is explored, i.e. several quantitative issues of our scheme are explored.

Keywords: Heart infarctions; Inverse problems; Level set techniques

1. Introduction

Millions of people in the Western world suffer from heart infarctions. The purpose of this paper is to explore the possibilities for using modern computers and mathematics to detect this disease. We will investigate whether the position, size and shape of heart infarctions can be computed from ECG measurements.

* Corresponding author. Tel.: +47 9589 5730.
E-mail addresses: bjornn@simula.no (B.F. Nielsen), mariul@simula.no (M. Lysaker), aslak@simula.no (A. Tveito).

0021-9991/$ - see front matter
doi:10.1016/j.jcp.2006.05.040

More specifically, our aim is to develop a suitable mathematical framework, expressed in terms of an inverse problem for a scalar partial differential equation (PDE), for doing so.

Ischemia, a precursor of heart infarction, is caused by an occlusion of one, or more, of the coronary arteries supplying blood to the myocardium. Consequently, the heart will not receive an adequate amount of blood and oxygen. If this condition persists, it may result in the death of the heart tissue, i.e. in an infarction. An ischemia may thus be viewed upon as a mild and reversible form of an infarction. We will throughout this paper, for the sake of convenience, use these two terms synonymously.

The electrical activity in the human body is usually modeled by the bidomain equations. This model consists of a nonlinear, fully coupled system of ordinary and partial differential equations. It is fairly easy to modify this framework to incorporate the effect of an infarction on the electrical field in the human body, see [3,4,26,32,34,35] for details. However, this complex system of equations is very hard to solve, and the simulation of the changes in the electrical potential throughout a single heart beat typically requires hours of computations, even on state-of-the-art parallel computers [33,36]. In the process of solving the associated inverse problem, i.e. the task of determining the physical characteristics of an ischemia from body surface measurements of the potential, the direct problem must be solved several times. This makes the traditional bidomain model unsuited for this kind of applications.

The purpose of the present paper is to show how biological knowledge about the transmembrane potential during rest (in the heart cycle) can be combined with level set techniques to define an efficient algorithm for computing the position and size of a myocardial infarction. It turns out that such an approach leads to a nonlinear minimization problem subject to a constraint defined in terms of a scalar elliptic PDE. Simulations performed with synthetic ECG data in 2D, on a standard modern laptop, indicate that the ischemic region can be identified within less than 3 min with this approach.

Several scientists have analyzed inverse problems arising in connection with ECG recordings. In particular, the challenge of how to compute the epicardial potential, i.e. the potential at the surface of the heart, based on body surface measurements has received a lot of attention, see [7,12,24,29] – to mention a few. The goal of such studies is to obtain a deeper understanding of this organ, including abnormal behavior due to some sort of illness. This approach, which will be referred to as the *classical inverse ECG problem*, has also, to some extent, been used to study ischemic heart disease [16,25]. More precisely, the presence of heart infarctions will in many cases be revealed through so-called ST shifts in the potential at the heart surface. Further details about this issue can be found in [14,23].

In many ways, our work is related to the results presented for the classical problem. However, from a mathematical and computational point of view, our approach is fundamentally different: Instead of seeking for indirect indications, for example in terms of ST shifts, of ischemic heart disease, we aim at directly computing the location and size of the infarction. That is, the unknowns in our framework are not the potential at specific locations at the heart surface, but parameters describing the physical characteristics of the ischemia itself. The mathematical formulations and properties, and consequently the applicability, of our framework is therefore fundamentally different from those of the classical inverse ECG problem.

As far as we know, Santosa [30] was the first researcher to apply level set methods to inverse obstacle problems. Throughout the last decade, such techniques have been applied to a wide range of applications of this kind; a nice survey is presented in [2]. Recently, this methodology has also been used to analyze inverse problems arising in connection with ECG recordings: In [21] a pilot study of how to use level set techniques to detect ischemic heart disease was discussed in terms of the so-called monodomain model, and [11] explains how the activation sequence at the heart surface may be computed in terms of level set techniques. The main purpose of the present paper is to derive a numerical method for automatically detecting ischemia and infarctions based on ECG-recordings. The actual implementation is described and prototypical numerical illustrations are provided. Further examples pursing biological issues are presented in [22].

This paper is organized as follows: The stationary forward model, including a discussion of how to use level set techniques to incorporate the effect of an ischemia, is presented in Section 2. Section 3 is devoted to the associated inverse problem, along with our main result; Algorithm 3.1. The performance, including important stability properties, of our scheme is studied through a series of numerical experiments in Section 4, and some concluding remarks are given in Section 5.

2. The forward model

As mentioned above, the electrical activity in the heart is modeled by the bidomain equations:

$$\frac{\partial s}{\partial t} = F(s,v) \quad \text{in } H, \tag{1}$$

$$\chi C v_t + \chi I(s,v) = \nabla\cdot(M_i\nabla v) + \nabla\cdot(M_i\nabla u_e) \quad \text{in } H, \tag{2}$$

$$\nabla\cdot(M_i\nabla v) + \nabla\cdot((M_i+M_e)\nabla u_e) = 0 \quad \text{in } H, \tag{3}$$

where (1) represents a system of ordinary differential equations (ODEs) and (2), (3) defines two partial differential equations (PDEs). Here, v and u_e denote the transmembrane and extra-cellular potentials, respectively, and H the physical domain occupied by the heart. The intra- and extra-cellular conductivity tensors M_i and M_e are typically defined in terms of symmetric and positive definite matrices depending on the spatial position x. Furthermore, I is a nonlinear function of both the transmembrane potential v and a state-vector s modeling the ionic concentrations in the heart. Since (3) will be the focus of this paper, we will not discuss the dependency of the state-vector s any further. The constants χ and C represent the area of cell membrane per unit volume and the capacitance of the cell membrane, respectively.

The bidomain equations (2) and (3) was introduced by Tung [37], and has been studied by several scientists, see [15,18,27,35] and references given therein. Many models for the cell-dynamics (1) have been proposed throughout the last three decades, see Beeler and Reuter [1], DiFrancesco [6], Luo and Rudy [19,20] and Winslow et al. [38].

In addition to (1)–(3), an equation governing the electrical potential in the remaining part of the body, i.e. outside the heart, must be specified. Furthermore, a set of suitable interface and boundary conditions at the heart and body surfaces must be included – leading to a complex system of equations. We will briefly return to these issues below.

As mentioned in the Introduction, in order to solve an inverse problem, the associated direct problem must typically be solved many times with different input parameters. The numerical computation of v, u_e and s from (1)–(3) is extremely CPU demanding, see [36] for details. The bidomain model is thus unfortunately not well-suited for the kind of application we are considering.

We will now show how the bidomain equations and biological knowledge can be combined to obtain a rather simple stationary model for the extra-cellular potential u_e during rest, and how the effect of an ischemia can be incorporated into this model with level set techniques. The inverse problem will be treated in Section 3.

The key point for deriving a stationary scalar equation for the extra-cellular potential u_e is that the transmembrane potential v is approximately known throughout the resting state/phase of the heart cycle. More precisely, v is approximately a piecewise constant function during rest. Furthermore, the properties of v are depending on whether or not ischemic tissues are present, cf. [3] for further details. Expressed in mathematical terms, this fact may be formulated as follows: Let t_1 be a time instance during the resting state of the heart cycle. According to lab measurements

$$v_1(x) = v(x,t_1) \approx \begin{cases} -60\ \text{mV} & x \text{ in ischemic tissue,} \\ -90\ \text{mV} & x \text{ in healthy tissue,} \end{cases} \tag{4}$$

see [17]. Consequently, (3) implies that the extra-cellular potential u_e at time $t = t_1$ must satisfy

$$\nabla\cdot((M_i+M_e)\nabla u_e(x,t_1)) = -\nabla\cdot(M_i\nabla v(x,t_1)) \quad \text{in } H, \tag{5}$$

where $v(x,t_1)$ is defined in (4).

Note that (5) only governs the potentials in the heart H. In order to obtain a complete model, an equation for the electrical activity outside the heart and suitable interface and boundary conditions at the heart and body surfaces must be specified.

Let B denote the domain, including the heart, occupied by the body, and define

$$T = B \setminus H,$$

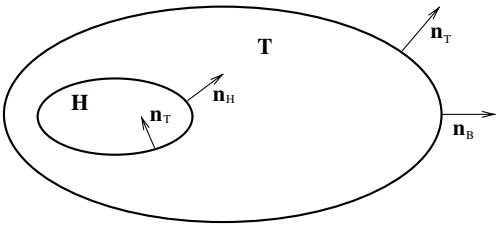

Fig. 1. A schematic of the body $B = H \cup T$. Note that $\partial T = \partial H \cup \partial B$, and that $\mathbf{n_T} = -\mathbf{n_H}$ along ∂H.

see Fig. 1. Since T is a passive conductor, the electrical activity in this part of the body is governed by an elliptic PDE:

$$\nabla \cdot (M_o \nabla u_o) = 0 \quad \text{in } T, \tag{6}$$

where M_o and u_o represent the conductivity and potential in T, respectively – see [35] for further details.

Throughout this paper we will assume that the body is insulated, leading to the boundary condition

$$(M_o \nabla u_o) \cdot \mathbf{n_B} = 0 \quad \text{along } \partial B, \tag{7}$$

where $\mathbf{n_B}$ denotes the outwards directed normal vector of unit length along the body surface ∂B. Next, the interface conditions for the potentials v, u_e and u_o along the heart surface ∂H are

$$u_e = u_o \quad \text{along } \partial H, \tag{8}$$

$$(M_e \nabla u_e) \cdot \mathbf{n_H} = -(M_o \nabla u_o) \cdot \mathbf{n_T} \quad \text{along } \partial H, \tag{9}$$

$$(M_i \nabla v + M_i \nabla u_e) \cdot \mathbf{n_H} = 0 \quad \text{along } \partial H, \tag{10}$$

see [35] for a discussion of these properties. In (9), $\mathbf{n_T}$ represents the outer unit normal vector of

$$\partial T = \partial H \cup \partial B,$$

cf. Fig. 1. Note that $\mathbf{n_T} = -\mathbf{n_H}$ along ∂H, and hence according to (9)

$$(M_e \nabla u_e) \cdot \mathbf{n_H} = (M_o \nabla u_o) \cdot \mathbf{n_H} \quad \text{along } \partial H.$$

The variational form of (5)–(7) and (8)–(10) can be derived in a rather straightforward manner. Let ψ be a test function defined on $B = H \cup T$. If we multiply (6) by ψ, integrate and apply Gauss' divergence theorem, we find that

$$\int_T \nabla\psi \cdot (M_o \nabla u_o)\,dx - \int_{\partial H} \psi (M_o \nabla u_o) \cdot \mathbf{n_T}\,ds = 0, \tag{11}$$

where we have used (7). In a similar manner, it follows from (3) that

$$\int_H \nabla\psi \cdot (M_i \nabla v)\,dx + \int_H \nabla\psi \cdot ((M_i + M_e)\nabla u_e)\,dx - \int_{\partial H} \psi (M_i \nabla v) \cdot \mathbf{n_H}\,ds - \int_{\partial H} \psi ((M_i + M_e)\nabla u_e) \cdot \mathbf{n_H}\,ds = 0. \tag{12}$$

Consequently, adding (11) and (12) and applying the interface conditions (8)–(10) imply that

$$\int_T \nabla\psi \cdot (M_o \nabla u_o)\,dx + \int_H \nabla\psi \cdot ((M_i + M_e)\nabla u_e) = -\int_H \nabla\psi \cdot (M_i \nabla v)\,dx \tag{13}$$

for every test function ψ defined throughout the entire body B.

If we introduce the notation

$$M(x) = \begin{cases} M_i(x) + M_e(x) & \text{for } x \in H, \\ M_o(x) & \text{for } x \in T, \end{cases}$$

and

$$u(x) = \begin{cases} u_e(x,t_1) & \text{for } x \in H, \\ u_o(x,t_1) & \text{for } x \in T, \end{cases}$$

we thus obtain the following model for the resting potential: Find $u \in V(B)$ such that

$$\int_B \nabla\psi \cdot (M\nabla u)\,dx = -\int_H \nabla\psi \cdot (M_i\nabla v_1)\,dx \quad \text{for all } \psi \in V(B), \tag{14}$$

where $v_1 = v(x,t_1)$ is (approximately) given in (4). In this formulation,

$$V(B) = \left\{\psi \in H^1(B); \int_B \psi\,dx = 0\right\}, \tag{15}$$

where $H^1(B)$ denotes the classical Sobolev space of functions defined on the domain B, see for example [9].

Remark I. Since the true membrane potential obeys, at least approximately, (4), it is important to check whether the bidomain model (1)–(3) generates solutions that satisfy this property. This can be viewed upon as a part of the validation process for such models. Fig. 2 shows the transmembrane potential v_1 during rest produced by (1)–(3). In this simulation a subendocardial anterior ischemia was incorporated into the equations by partially removing the ion transport in the ischemic tissue, see [35]. The cell dynamics were modeled by the method proposed by Winslow et al., see [38]. According to this plot, such models indeed produce membrane potentials that are consistent with (4) – at least in an approximate sense. Our goal is to investigate the possibilities for exploiting this property to identify ischemic heart disease. More precisely, to determine the position and size of an ischemia.

Remark II. The function v_1, as approximately defined in (4), is discontinuous along the interface separating the healthy and ischemic tissues in the heart. In the model (14), the partial derivatives of v_1 are present. It is by no means straightforward to define the derivative of functions of this kind; it represents a subtle mathematical challenge. On the other hand, from a biological point of view, the border zone between the healthy and damaged tissue should not be represented by a sharp discontinuity in v_1. More accurate models include a smooth transition zone between such regions, see [31]. This is also in agreement with the plot presented in Fig. 2. This matter will be treated with level set techniques and approximate Heaviside functions in Section 2.1.

A similar discussion applies to the unknown function u in (14). If v_1 or the conductivities M_i, M_e, M_o are discontinuous, then there might not exist any solution u of (14) or this function might only posses a low order of regularity. However, as will be explained below, by applying smooth approximations of the Heaviside function in the modeling process of v_1 and the conductivities, it follows from standard theory for elliptic PDEs, see e.g. [9], that there exist a solution $u \in V(B) \subset H^1(B)$. Note that this also implies that ∇u is well-behaved throughout the body B.

Please note that, for the sake of simplicity, we will drop the subscript "1" in v_1 and simply let v denote the transmembrane potential during rest.

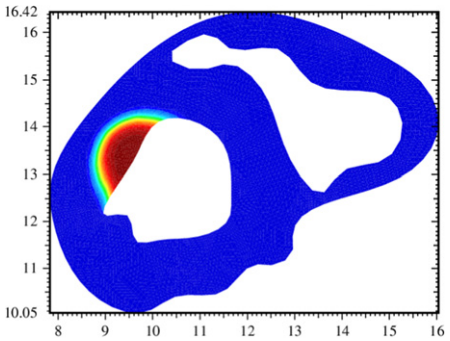

Fig. 2. The transmembrane potential v_1 during rest generated by the bidomain model.

2.1. Incorporating ischemia

The purpose of this section is to explain how level set techniques can be used to incorporate the effect of one, or more, infarctions into the model (14). To this end, let $D \subset H$ denote the domain occupied by the ischemic region(s) in the heart, and recall that during rest

$$v(x) \approx \begin{cases} a_1 & \text{for } x \text{ in } D, \\ a_2 & \text{for } x \text{ in } H \setminus D. \end{cases} \tag{16}$$

where $a_1 = -60$ mV and $a_2 = -90$ mV, see (4). From a mathematical point of view, it turns out to be convenient to assume that D is an open set.

As already mentioned above, biological considerations indicate that the interface between the healthy and damaged tissue in the heart should not be implemented in terms of a jump discontinuity in the membrane potential v. In realistic models, this interface must be incorporated by a smooth transition zone. To accomplish for such an effect, we will throughout this paper use approximations of the Heaviside function G:

$$G(s) = \begin{cases} 0 & \text{for } s < 0, \\ 1 & \text{for } s \geqslant 0. \end{cases}$$

More precisely, consider the family of smooth approximations $G_\tau \approx G$, where τ is a positive parameter,

$$G_\tau(s) = \begin{cases} 1 & \text{if } s > \tau, \\ 0 & \text{if } s < -\tau, \\ \frac{1}{2}\left[1 + \frac{s}{\tau} + \frac{1}{\pi}\sin\left(\frac{\pi s}{\tau}\right)\right] & \text{if } |s| \leqslant \tau. \end{cases} \tag{17}$$

Then, by introducing a level set function $\phi : H \to \mathbb{R}$ with the property

$$\phi(x) < 0 \quad \text{if } x \in D, \tag{18}$$

$$\phi(x) = 0 \quad \text{if } x \in \partial D, \tag{19}$$

$$\phi(x) > 0 \quad \text{if } x \in H \setminus \overline{D}, \tag{20}$$

we may model the transmembrane potential during rest with the formula

$$v = v(\phi) = v(\phi;\tau) = a_1[1 - G_\tau(\phi)] + a_2 G_\tau(\phi), \tag{21}$$

see (16).

For a given domain D, there are of course infinitely many functions ϕ satisfying (18)–(20). We will, as is usual in the level set literature, define ϕ in terms of the distance to the boundary ∂D of D:

$$\phi(x) = -\text{dist}(\partial D, x) \quad \text{if } x \in D, \tag{22}$$

$$\phi(x) = 0 \quad \text{if } x \in \partial D, \tag{23}$$

$$\phi(x) = \text{dist}(\partial D, x) \quad \text{if } x \in H \setminus \overline{D}, \tag{24}$$

where $\text{dist}(\partial D, x)$ is the Euclidean distance between ∂D and x. There are several, in particular algorithmic, reasons for using functions on form (22)–(24). We will not dwell any further upon this topic, further details can be found in [28].

The smoothness, as it is represented in v in (21), of the transition zone between the healthy and ischemic regions is dominated by the parameter τ, cf. (17). Furthermore, the derivatives of $v_1 = v$ occur at the right hand side of (14). This means that τ plays an important role in the present model. We will return to this issue in Section 4.

Please note that (17) provides a family $\{\delta_\tau\}_{\tau>0}$ of approximate Delta functions:

$$\delta_\tau(s) = G'_\tau(s) = \begin{cases} 0 & \text{if } |s| > \tau, \\ \frac{1}{2\tau}\left[1 + \cos\left(\frac{\pi s}{\tau}\right)\right] & \text{if } |s| \leqslant \tau, \end{cases} \tag{25}$$

with derivatives

$$\delta'_\tau(s) = G''_\tau(s) = \begin{cases} 0 & \text{if } |s| > \tau, \\ -\frac{\pi}{2\tau^2}\sin\left(\frac{\pi s}{\tau}\right) & \text{if } |s| \leqslant \tau, \end{cases} \tag{26}$$

2.1.1. Conductivities

In the framework presented above, the effect of the ischemia on the extra-cellular potential was included in our model by assigning the transmembrane potential v the approximately piecewise constant property expressed in Eq. (21). However, the intra- and extra-cellular conductivities M_i and M_e will also depend on whether or not ischemic tissue is present, see [13] for details. Consequently, this phenomena should ideally be incorporated into the equations.

In mathematical models of the electrical activity of the heart, the conductivities M_i and M_e are typically defined in terms of spatially dependent matrices. More specifically, in healthy tissue,

$$M_\mathrm{i} = \sigma_\mathrm{i}^\mathrm{t}\mathbf{I} + (\sigma_\mathrm{i}^\mathrm{l} - \sigma_\mathrm{i}^\mathrm{t})\mathbf{a}_\mathrm{l}\mathbf{a}_\mathrm{l}^\mathrm{T} + (\sigma_\mathrm{i}^\mathrm{n} - \sigma_\mathrm{i}^\mathrm{t})\mathbf{a}_\mathrm{n}\mathbf{a}_\mathrm{n}^\mathrm{T}, \tag{27}$$

$$M_\mathrm{e} = \sigma_\mathrm{e}^\mathrm{t}\mathbf{I} + (\sigma_\mathrm{e}^\mathrm{l} - \sigma_\mathrm{e}^\mathrm{t})\mathbf{a}_\mathrm{l}\mathbf{a}_\mathrm{l}^\mathrm{T} + (\sigma_\mathrm{e}^\mathrm{n} - \sigma_\mathrm{e}^\mathrm{t})\mathbf{a}_\mathrm{n}\mathbf{a}_\mathrm{n}^\mathrm{T}, \tag{28}$$

where $\mathbf{a}_\mathrm{l} = \mathbf{a}_\mathrm{l}(x)$ and $\mathbf{a}_n = \mathbf{a}_n(x)$ are vectors incorporating the fiber structure of the myocardium in the longitudinal and transverse directions, respectively, and $\sigma_\mathrm{i}^\mathrm{l}$, $\sigma_\mathrm{i}^\mathrm{n}$ and $\sigma_\mathrm{i}^\mathrm{t}$ are scalars [35]. According to the bioengineering literature, the vector functions $\mathbf{a}_\mathrm{l}$ and $\mathbf{a}_n$ are independent of whether or not ischemic tissue is present, see e.g. [10,14]. This is not the case for the parameters $\sigma_\mathrm{i}^\mathrm{l}$, $\sigma_\mathrm{i}^\mathrm{n}$ and $\sigma_\mathrm{i}^\mathrm{t}$. They will change in the damaged areas, see Table 1, leading to different intra- and extra-cellular conductivities in such regions:

$$S_\mathrm{i} = \widetilde{\sigma}_\mathrm{i}^\mathrm{t}\mathbf{I} + (\widetilde{\sigma}_\mathrm{i}^\mathrm{l} - \widetilde{\sigma}_\mathrm{i}^\mathrm{t})\mathbf{a}_\mathrm{l}\mathbf{a}_\mathrm{l}^\mathrm{T} + (\widetilde{\sigma}_\mathrm{i}^\mathrm{n} - \widetilde{\sigma}_\mathrm{i}^\mathrm{t})\mathbf{a}_\mathrm{n}\mathbf{a}_\mathrm{n}^\mathrm{T}, \tag{29}$$

$$S_\mathrm{e} = \widetilde{\sigma}_\mathrm{e}^\mathrm{t}\mathbf{I} + (\widetilde{\sigma}_\mathrm{e}^\mathrm{l} - \widetilde{\sigma}_\mathrm{e}^\mathrm{t})\mathbf{a}_\mathrm{l}\mathbf{a}_\mathrm{l}^\mathrm{T} + (\widetilde{\sigma}_\mathrm{e}^\mathrm{n} - \widetilde{\sigma}_\mathrm{e}^\mathrm{t})\mathbf{a}_\mathrm{n}\mathbf{a}_\mathrm{n}^\mathrm{T}. \tag{30}$$

Recall that we introduced the symbol D to denote the domain occupied by the ischemic region(s). By applying the approximate Heaviside function defined in (17), we now may introduce ischemic dependent conductivities K_i and K_e with the formulas

$$\begin{aligned} K_\mathrm{i}(\phi) &= S_\mathrm{i}[1 - G_\alpha(\phi)] + M_\mathrm{i}G_\alpha(\phi), \\ K_\mathrm{e}(\phi) &= S_\mathrm{e}[1 - G_\alpha(\phi)] + M_\mathrm{e}G_\alpha(\phi), \end{aligned} \tag{31}$$

where ϕ is the level set function in (22)–(24). In general $\alpha \neq \tau$, (see (21)), meaning that the smoothing parameters for the conductivities and membrane potentials may be different. Note that

$$K_\mathrm{i}(\phi(x)) \approx \begin{cases} S_\mathrm{i}(x) & \text{for } x \text{ in } D, \\ M_\mathrm{i}(x) & \text{for } x \text{ in } H \setminus D, \end{cases} \tag{32}$$

and

$$K_\mathrm{e}(\phi(x)) \approx \begin{cases} S_\mathrm{e}(x) & \text{for } x \text{ in } D, \\ M_\mathrm{e}(x) & \text{for } x \text{ in } H \setminus D, \end{cases} \tag{33}$$

provided that $\alpha > 0$ is small.

Table 1
Conductivity values for healthy and ischemic tissues as reported in [10,14]

Conductivity	Value (in mS/cm)
Healthy intra-cellular longitudinal, $\sigma_\mathrm{i}^\mathrm{l}$	3.0
Healthy intra-cellular transverse, $\sigma_\mathrm{i}^\mathrm{t}$	0.31525
Healthy extra-cellular longitudinal, $\sigma_\mathrm{e}^\mathrm{l}$	2.0
Healthy extra-cellular transverse, $\sigma_\mathrm{e}^\mathrm{t}$	1.3514
Ischemic intra-cellular longitudinal, $\widetilde{\sigma}_\mathrm{i}^\mathrm{l}$	3.0
Ischemic intra-cellular transverse, $\widetilde{\sigma}_\mathrm{i}^\mathrm{t}$	0.31525
Ischemic extra-cellular longitudinal, $\widetilde{\sigma}_\mathrm{e}^\mathrm{l}$	1.0
Ischemic extra-cellular transverse, $\widetilde{\sigma}_\mathrm{e}^\mathrm{t}$	0.5

Finally, by putting

$$K(\phi(x)) = \begin{cases} K_{\mathrm{i}}(\phi(x)) + K_{\mathrm{e}}(\phi(x)), & \text{for } x \text{ in } H, \\ M_{\mathrm{o}}(x), & \text{for } x \text{ in } T, \end{cases} \tag{34}$$

we may introduce the following modified version of (14): Find $u \in V(B)$ such that

$$\int_B \nabla\psi \cdot (K\nabla u)\,\mathrm{d}x = -\int_H \nabla\psi \cdot (K_{\mathrm{i}}\nabla v)\,\mathrm{d}x, \quad \forall\psi \in V(B), \tag{35}$$

where v is the transmembrane potential defined in (21), and K_{i} and K are defined in (31) and (34), respectively.

Eq. (35) concludes our derivation of the forward problem: Suppose the characteristics of the ischemic region(s) are known. Then, as explained above, the transmembrane potential, as well as the conductivities, are approximately given; see (21), (31) and (34). Consequently, the effect of the infarction(s) on the body surface potential may be determined by solving (35) for u, i.e. the impact of the ischemia on the ECG signal during rest can be computed. However, we are mainly interested in the associated inverse problem. That is, with the challenge of how to use measured body surface potentials to determine the position, size and shape of the ischemic region(s).

3. Identifying ischemia, an inverse problem

Let d denote the measured resting potential at the body surface, i.e. $d : \partial B \to \mathbb{R}$ is a given function representing the available observation data.[1] Note that the ischemic area D satisfies

$$D = \{x; \phi(x) < 0\}, \tag{36}$$

see (22)–(24). Hence, if we can use our observation data d and the model (35) to determine ϕ, then it follows that the infarcted region(s) can be identified with (36).

Formulas (31), (34) and (21) imply that the conductivities K_{i}, K_{e} and K, as well as the membrane potential v, depend on ϕ. Consequently, the solution u of (35) will also be a function of ϕ, $u = u(x;\phi)$. We may thus use the output least squares method to (approximately) identify ϕ:

$$\min_{\phi} \|u(\phi) - d\|^2_{L^2(\partial B)} \tag{37}$$

subject to $u = u(\phi)$ satisfying (35). This infinite dimensional minimization problem is of course hard to solve. We will thus discretize (37) and handle it by numerical techniques.

Let $\{N_i\}_{i=1}^M$ denote a set of finite element basis functions defined throughout the heart H, and consider the discrete level set function

$$\phi(x) = \sum_{i=1}^{M} p_i N_i(x). \tag{38}$$

With this notation at hand, we may define the following approximation of (37):

$$\min_{p_1,p_2,\ldots,p_M} J(p_1, p_2, \ldots, p_M), \tag{39}$$

where

$$J(p_1, p_2, \ldots, p_M) = \frac{1}{2}\int_{\partial B} [u(x; p_1, p_2, \ldots, p_M) - d(x)]^2\,\mathrm{d}x. \tag{40}$$

Throughout this paper, $p_1, p_2, \ldots, p_M$ will be referred to as the *infarction parameters*. Note that, since u is a function of ϕ, u depends on $p_1, p_2, \ldots, p_M$

[1] Traditional ECG devices only record the potential at specific locations, referred to as the lead positions. We will not dwell any further on this practical aspect of the present problem, and simply assume that the potential is measured at the entire body surface.

$$u = u(x;\phi) = u(x;p_1,p_2,\ldots,p_M).$$

Our next goal is to construct an algorithm suitable for solving (39).

3.1. Differentiation of the cost-functional

Many minimization methods require the partial derivatives of the involved cost-functional. Let us therefore show how $\partial J/\partial p_1, \partial J/\partial p_2, \ldots, \partial J/\partial p_M$ can be computed efficiently in terms of the adjoint problem approach. To this end, we will assume that all the involved derivatives exist and are well-behaved, and thus proceed in a rather formal manner.

Let $j \in \{1,2,\ldots,M\}$ be arbitrary. From (40) we find that

$$\frac{\partial J}{\partial p_j} = \int_{\partial B} [u(x;p_1,p_2,\ldots,p_M) - d(x)] u_{p_j}(x;p_1,p_2,\ldots,p_M)\,\mathrm{d}x. \tag{41}$$

Note that differentiation of (35) with respect to p_j yields

$$\begin{aligned}&\int_B \nabla\psi\cdot[K'(\phi)\phi_{p_j}\nabla u]\,\mathrm{d}x + \int_B \nabla\psi\cdot[K(\phi)\nabla u_{p_j}]\,\mathrm{d}x\\ &\quad = -\int_H \nabla\psi\cdot[K_{\mathrm{i}}'(\phi)\phi_{p_j}\nabla v(\phi)]\,\mathrm{d}x - \int_H \nabla\psi\cdot[K_{\mathrm{i}}(\phi)\nabla v_{p_j}(\phi)]\,\mathrm{d}x,\end{aligned} \tag{42}$$

or

$$\begin{aligned}\int_B \nabla\psi\cdot[K(\phi)\nabla u_{p_j}]\,\mathrm{d}x = &-\int_B \nabla\psi\cdot[K'(\phi)\phi_{p_j}\nabla u]\,\mathrm{d}x - \int_H \nabla\psi\cdot[K_{\mathrm{i}}'(\phi)\phi_{p_j}\nabla v(\phi)]\,\mathrm{d}x\\ &- \int_H \nabla\psi\cdot[K_{\mathrm{i}}(\phi)\nabla v_{p_j}(\phi)]\,\mathrm{d}x\end{aligned} \tag{43}$$

for all $\psi \in V(B)$. If we introduce the operator

$$a(\xi,\psi) = \int_B \nabla\psi\cdot[K(\phi)\nabla\xi]\,\mathrm{d}x \quad \text{for } \xi,\psi \in V(B), \tag{44}$$

Eq. (43) may be written on the form

$$a(u_{p_j},\psi) = -\int_B \nabla\psi\cdot[K'(\phi)\phi_{p_j}\nabla u]\,\mathrm{d}x - \int_H \nabla\psi\cdot[K_{\mathrm{i}}'(\phi)\phi_{p_j}\nabla v(\phi)]\,\mathrm{d}x - \int_H \nabla\psi\cdot[K_{\mathrm{i}}(\phi)\nabla v_{p_j}(\phi)]\,\mathrm{d}x \tag{45}$$

for all $\psi \in V(B)$. Furthermore, $u \in V(B)$ imply that $u_{p_j} \in V(B)$, see (15).

Next, let w denote the solution of the following auxiliary problem: Find $w \in V(B)$ such that

$$a(\psi,w) = \int_{\partial B} [u(x;p_1,p_2,\ldots,p_M) - d(x)]\psi\,\mathrm{d}x \tag{46}$$

for all $\psi \in V(B)$. By choosing $\psi = u_{p_i}$ in (46) we find from (41) that

$$\frac{\partial J}{\partial p_j} = a(u_{p_j},w). \tag{47}$$

Moreover, (45) and (47) imply that

$$\frac{\partial J}{\partial p_j} = -\int_B \nabla w\cdot[K'(\phi)\phi_{p_j}\nabla u]\,\mathrm{d}x - \int_H \nabla w\cdot[K_{\mathrm{i}}'(\phi)\phi_{p_j}\nabla v(\phi)]\,\mathrm{d}x - \int_H \nabla w\cdot[K_{\mathrm{i}}(\phi)\nabla v_{p_j}(\phi)]\,\mathrm{d}x. \tag{48}$$

Next, from (31) and (34) it follows that

$$\begin{aligned}K_{\mathrm{i}}'(\phi) &= -S_{\mathrm{i}}\delta_\alpha(\phi) + M_{\mathrm{i}}\delta_\alpha(\phi) = (M_{\mathrm{i}} - S_{\mathrm{i}})\delta_\alpha(\phi),\\ K_{\mathrm{e}}'(\phi) &= -S_{\mathrm{e}}\delta_\alpha(\phi) + M_{\mathrm{e}}\delta_\alpha(\phi) = (M_{\mathrm{e}} - S_{\mathrm{e}})\delta_\alpha(\phi),\end{aligned} \tag{49}$$

and

$$K'(\phi) = \begin{cases} K'_{\mathrm{i}}(\phi) + K'_{\mathrm{e}}(\phi), & \text{for } x \text{ in } H, \\ 0, & \text{for } x \text{ in } T. \end{cases} \tag{50}$$

Furthermore, from (21) we see that

$$v_{p_j}(\phi) = (a_2 - a_1)\delta_\tau(\phi)\phi_{p_j}, \tag{51}$$

whereupon

$$\nabla v_{p_j}(\phi) = (a_2 - a_1)[\nabla\delta_\tau(\phi)\phi_{p_j} + \delta_\tau(\phi)\nabla\phi_{p_j}]. \tag{52}$$

Consequently, inserting (50) and (52) into (48) provides the formula

$$\begin{aligned} \frac{\partial J}{\partial p_j} = &- \int_H \nabla w \cdot [M_{\mathrm{i}} - S_{\mathrm{i}} + M_{\mathrm{e}} - S_{\mathrm{e}}]\delta_\alpha(\phi)\phi_{p_j}\nabla u \,\mathrm{d}x - \int_H \nabla w \cdot [M_{\mathrm{i}} - S_{\mathrm{i}}]\delta_\alpha(\phi)\phi_{p_j}\nabla v(\phi)\,\mathrm{d}x \\ &- (a_2 - a_1)\int_H \nabla w \cdot K_{\mathrm{i}}(\phi)[\nabla\delta_\tau(\phi)\phi_{p_j} + \delta_\tau(\phi)\nabla\phi_{p_j}]\,\mathrm{d}x, \end{aligned} \tag{53}$$

where

$$\nabla\delta_\tau(\phi) = \delta'_\tau(\phi)\nabla\phi.$$

A few comments are in place:

(1) The key point of this analysis is that all the partial derivatives $\partial J/\partial p_1, \partial J/\partial p_2, \ldots, \partial J/\partial p_M$ of J can be computed by solving a single auxiliary problem on the form (46). If this task was to be accomplished in terms of finite differences, one would typically have to solve M elliptic forward problems (35) with slightly perturbed parameters. For large values of M, such an approach would lead to extremely CPU demanding algorithms, even exceeding the computing power of modern mainframes.
(2) Interestingly, $\partial J/\partial p_j$ for $j = 1,2,\ldots,M$ is given in terms of integrals over the heart H, see (53). By and large, the properties of u and w in $T = B\backslash H$, cf. Fig. 1, do not matter for the computation of the partial derivatives! In fact, a more detailed analysis would reveal that these partial derivatives are fully determined by the behavior of the involved functions in the vicinity of the interface ∂D. This follows from basic properties of v, see (21), (17), (25) and (26). Our observations are thus in accordance with those presented in [30].
(3) By assuming that all the involved functions are sufficiently well-behaved, one can show that the classical form of the adjoint problem (46) reads

$$\nabla \cdot [K(\phi)\nabla w] = 0 \quad \text{in } B, \tag{54}$$

$$K(\phi)\nabla w \cdot n = u - c - d \quad \text{along } \partial B, \tag{55}$$

$$\int_B w\,\mathrm{d}x = 0, \tag{56}$$

where $c = \int_{\partial B}(u - d)\,\mathrm{d}x$.

3.2. An algorithm

Let us now consider the algorithmic aspects of the theoretical considerations presented above. More precisely, we will define a simple iterative scheme suitable for (approximately) solving (39).

For the sake of convenience, let us introduce the notation

$$\mathbf{p} = (p_1, p_2, \ldots, p_M)^{\mathrm{T}}$$

for the infarction parameters, cf. (38). Next, let $\mathbf{p}^n = (p_1^n, p_2^n, \ldots, p_M^n)^{\mathrm{T}}$ denote the nth approximation of the solution of (39) generated by our method and define

$$\phi^n = \phi(\mathbf{p}^n) = \sum_{i=1}^{M} p_i^n N_i. \tag{57}$$

With this notation at hand, we define the following algorithm:

Algorithm 3.1

(1) Choose appropriate values for α and τ to use in the approximate Heaviside functions G_α and G_τ, cf. (17), (21) and (31)
(2) Choose a diagonal matrix $\mathbf{B} = \mathrm{diag}(\beta_1, \beta_2, \ldots, \beta_M)$ to use in step 4(d) below
(3) Choose an initial guess $\mathbf{p}^0$ for the infarction parameters
(4) For $n = 0, 1, \ldots$ until convergence do
  (a) Solve (35) for $u^n = u(\phi^n)$
  (b) Solve (46) for $w^n = w(\phi^n)$
  (c) Compute

$$\frac{\partial J}{\partial p_j}(\mathbf{p}^n) = -\int_H \nabla w^n \cdot [M_\mathrm{i} - S_\mathrm{i} + M_\mathrm{e} - S_\mathrm{e}]\delta_\alpha(\phi^n)\phi^n_{p_j}\nabla u^n \,\mathrm{d}x - \int_H \nabla w^n \cdot [M_\mathrm{i} - S_\mathrm{i}]\delta_\alpha(\phi^n)\phi^n_{p_j}\nabla v(\phi^n)\,\mathrm{d}x$$
$$- (a_2 - a_1)\int_H \nabla w^n \cdot K_\mathrm{i}(\phi^n)[\nabla\delta_\tau(\phi^n)\phi^n_{p_j} + \delta_\tau(\phi^n)\nabla\phi^n_{p_j}]\,\mathrm{d}x,$$

  for $j = 1, \ldots, M$.
  (d) Define

$$\mathbf{p}^{n+1} = \mathbf{p}^n - \mathbf{B}\nabla J(\mathbf{p}^n), \tag{58}$$
$$\text{where } \nabla J(\mathbf{p}^n) = (\partial J/\partial p_1(\mathbf{p}^n), \ldots, \partial J/\partial p_M(\mathbf{p}^n))^\mathrm{T}$$

This is a Landweber type of scheme, see e.g. [8]. Note that we use a diagonal matrix $\mathbf{B}$ instead of a scalar in step 4(d). This is due to the fact that the size of the partial derivatives $\{\partial J/\partial p_j\}$ depend heavily on j. More specifically, numerical experiments indicate that, in general, $\partial J/\partial p_j$ is much larger for indices $\{j\}$ associated with nodes positioned at the surface ∂H of the heart H than for internal nodes. In the examples presented in Section 4, $\mathbf{B} = \mathrm{diag}(\beta_1, \beta_2, \ldots, \beta_M)$ is defined as follows:

$$\beta_j = \begin{cases} \beta & \text{if } j \text{ is associated with a node inside } H, \\ \beta_{\partial H} & \text{if } j \text{ is associated with a node at } \partial H, \end{cases} \tag{59}$$

where $\beta > \beta_{\partial H} > 0$ are scalars. Furthermore, β and $\beta_{\partial H}$ were determined by the trial end error "method". (Clearly, more advanced optimization techniques, such as e.g. a line-search strategy or (quasi) Newton schemes, could have been applied to solve (39). However, that topic is beyond the scope of the present paper).

In the examples presented below we use a "healthy" heart, i.e. no ischemia, as the initial guess in Algorithm 3.1. This means that $p_i^0 > 0$ for $i = 1, 2, \ldots, M$ and hence $\phi^0(x) > 0$ for all $x \in H$, cf. (57). Please note the following: If we had used exact delta functions in Algorithm 3.1, then all the corrections computed in step (4) would have been zero. Consequently, $\mathbf{p}^n = \mathbf{p}^0$ for $n = 1,2,3,\ldots$ However, the approximate delta functions prevent this from happening, and makes it possible to use a "healthy" heart as initial guess.

4. Numerical experiments

This section is devoted to an experimental study of Algorithm 3.1. As mentioned above, we will investigate the role of the smoothing parameter τ used in the approximate Heaviside function G_τ, and how noisy data influences the behavior of our scheme.

All simulations used the 2D geometry shown in Fig. 3(a). The anisotropic cardiac conductivity values are given in Table 1, and the fiber directions within the heart are depicted in Fig. 3(b). If not specified otherwise, the computational grid consisted of 18433 nodes (4059 in the heart) and 36448 elements (7488 in the heart).

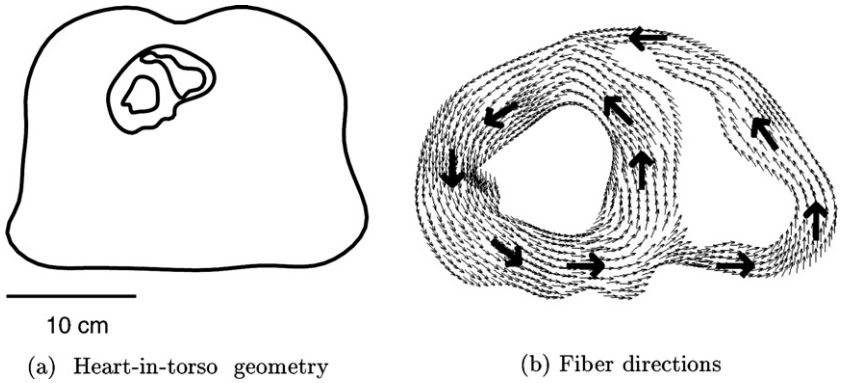

Fig. 3. The geometry (a) and fiber structure (b) used in the computations.

In all the experiments the observation data d, cf. (37), was produced by the following procedure:

- An ischemic zone D was "inserted" into the heart H by altering the cell dynamics and conductivities in this region.
- The bidomain model (1)–(3), using the Winslow et al. cell model [38], was solved.
- The observation data d was set equal to the body surface potential during rest generated by the bidomain simulation.

This means that the set of equations used to generate synthetic values for d was different from the model applied to solve the inverse problem. Consequently, so-called "inverse crimes" [5] were avoided. Further details about bidomain simulations can be found in [35].

In order to apply Algorithm 3.1, appropriate values for the smoothing parameters τ and α, cf. Eqs. (17)–(21) and (27)–(31), must be chosen. This was accomplished in the following way: Let v_1 denote the transmembrane potential during rest generated by the bidomain model (1)–(3), see Fig. 2, and recall the "Ansatz" (21) for the function $v(\phi;\tau)$ used in the stationary forward model (35). Then we define an "optimal/feasible" value τ^* for τ by

$$\tau^* = \operatorname*{argmin}_{\tau} \|v_{\mathrm{bi}} - v(\phi_{\mathrm{true}};\tau)\|_{L^2(H)}, \tag{60}$$

where ϕ_{true} denotes the level set function associated with the true infarction. Except for the results presented in Example II below, we used $\alpha = \tau = \tau^*$ in all our experiments.

As mentioned above, in all the tests we used a "healthy" heart, i.e. no infarction, as initial guess $\mathbf{p}^0$ in the iteration (58).

Example I. In order to illuminate the convergence properties of Algorithm 3.1, we have in Fig. 4 plotted the true ischemia along with approximations of it generated by 3, 20 and 43 iterations of the scheme. These plots were generated with noise free observation data d (cases involving noise will be presented in Example III).

According to this figure, only a few iterations are needed to roughly identify the position of the damaged tissue. And, approximately 20 iterations provide a rather good approximation of the size of the ischemia. However, the convergence speed seems to slow down considerably after 20 iterations; compare Fig. 4(c) and (d).

Fig. 5 shows the relative error in the center of mass (CM) of the estimated ischemia and the cost-functional J, defined in (40), as functions of the number of iteration used in Algorithm 3.1. More precisely, the relative error in CM is computed according to the formula

$$\frac{|\text{CM of true ischemia} - \text{CM of estimated ischemia}|}{6.7\ \text{cm}}, \tag{61}$$

where 6.7 cm approximately is the cubic root of 300 cm^3, which is a typical heart volume.

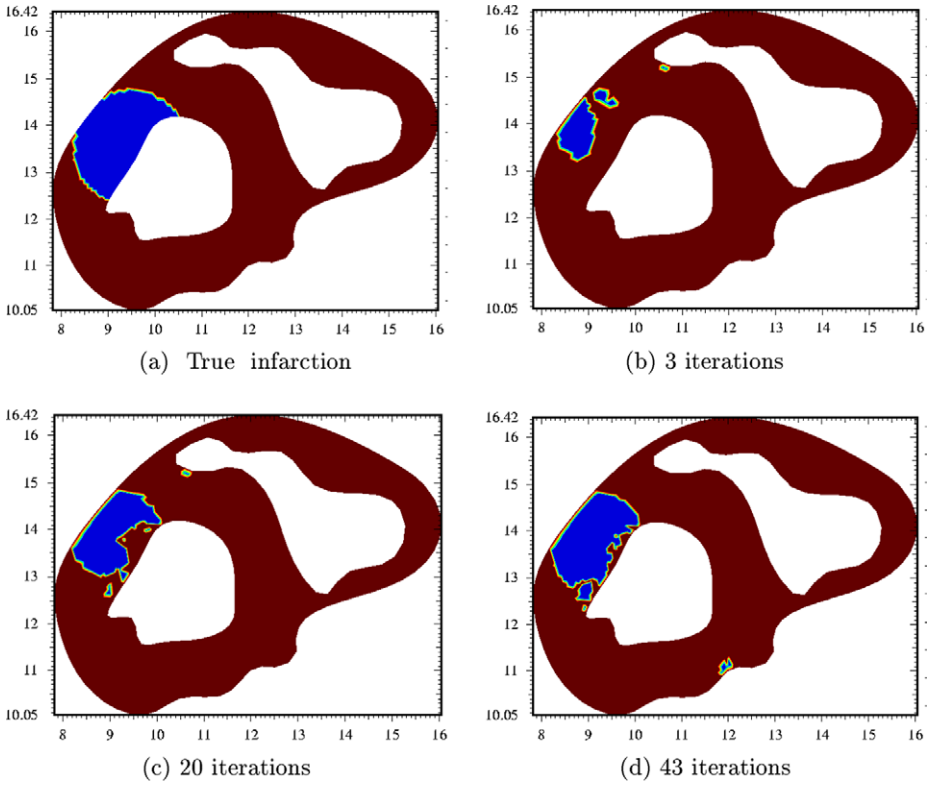

Fig. 4. The infarction we try to identify is shown in (a). The result obtained with 3, 20, and 43 iterations of Algorithm 3.1 are presented in figures (b)–(d), respectively.

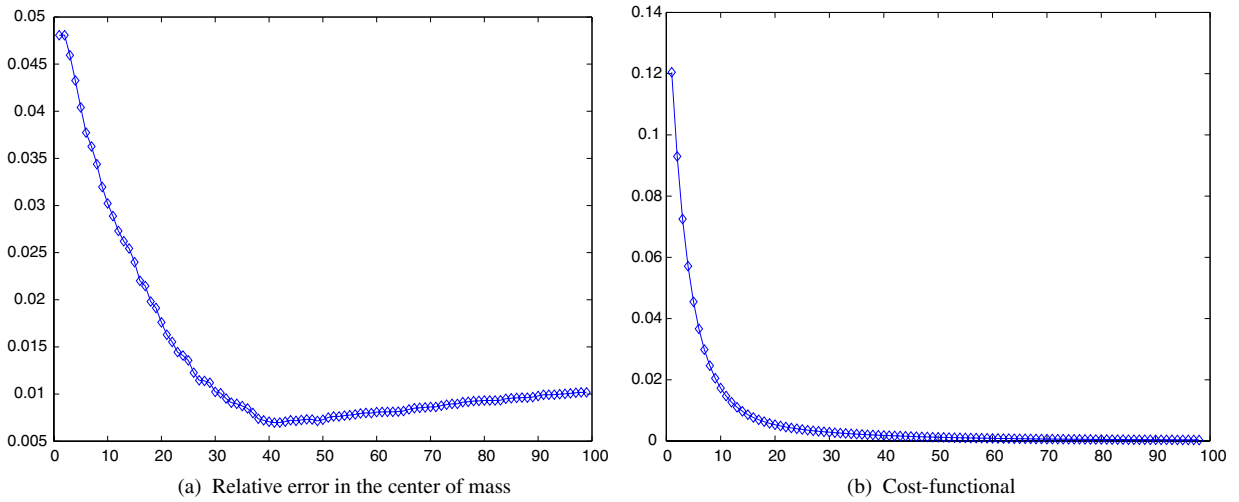

Fig. 5. Plots of the relative error in the center of mass (a) and the cost-functional J (b) as functions of the number of iterations in Algorithm 3.1.

Fig. 5(a) shows that the least error in the center of mass is reached after 43 iterations; performing more than 43 iterations will only deteriorate our result. On the other hand, the residual, i.e. the value of our cost-functional J, decreases monotonically with the number of iterations, see Fig. 5(b). These plots thus clearly illuminate the ill-posed nature of the problem at hand; it is in general "impossible" to compute a sequence of

approximate solutions that will converge towards the true solution, we must be content with ''rather rough'' estimates of the ischemia. (Note that this is even the case for noise free observation data d

Table 3
Results obtained with noisy observation data d_η, where $0 \leqslant \eta \leqslant 2\%$

Noise η (%)	Discrepancy		Manually	
	Error CM (%)	Error area (%)	Error CM (%)	Error area (%)
0.0	–	–	0.7	16.2
0.5	3.0	19.9	1.6	22.7
1.0	4.1	31.0	2.1	27.4
1.5	4.5	38.4	2.9	34.4
2.0	5.0	42.5	3.0	34.1

The table shows *averages* obtained by running our scheme 20 times for each noise level.

center of mass (in practical situations such a technique is of course not applicable; it requires detailed knowledge about the true solution).

The averaging used to generate the numbers presented in Table 3 could be a little dangerous, since in practical situations only a very limited number of observations are available,[2] and certain errors may get averaged out by computing mean values. Therefore, the worst results among the 20 simulations used to produce the numbers in Table 3 are presented in Table 4.

According to these tables, the center of mass (CM) is estimated accurately. Except for some of the worst-case results obtained with the discrepancy principle, the error in the area of the ischemia is approximately one magnitude larger than the error in the CM. For noise levels $\eta \leqslant 2\%$, the algorithm correctly recovered the region in which the infarction occurred (not suggesting any ischemia in positions with healthy tissue). In average, the discrepancy principle handled this problem fairly nice; compare the columns entitled "Discrepancy" and "Manually" in Table 3. On the other hand, the worst-case results for the CM generated with this principle are of a surprisingly low quality compared with the averages, see Table 4.

For $\eta \geqslant 3\%$ the scheme did not necessary correctly identify the right location of the infarction; in some of the 20 runs of the algorithm, it thus happened that healthy tissue was incorrectly classified as ischemic regions. In Table 5 we have consequently included the so-called "detection rate", referring to how many of the 20 runs that were successful. The errors in the CM and area presented in this table are averages computed from the successful cases.

In addition to the quantitative issues reported in Tables 3–5, we have also included qualitative results in Fig. 6. More specifically, this figure shows the true infarction along with typical[3] estimates provided by our algorithm, applying the discrepancy principle to stop the iteration, in the case of 1%, 3% and 5% noise in the observation data. Note that the size of the ischemia is underestimated. This observation was made in a number of cases; it seems that the discrepancy principle defines a too strict stopping criteria for our algorithm. Roughly speaking, this technique works well for identifying the position of the ischemia but not that well for estimating its size. From a clinical point of view, it is not clear which of these properties that are most important: The position provides information about which of the arteries that are occluded, whereas the size is connected to the severity of the disease. This matter should be explored in more detail. However, it is a delicate issue and deserves a thorough investigation, which is beyond the scope of the present paper.

Based on the results presented in Tables 3–5 and Fig. 6, it seems to be reasonable to conclude that our scheme is capable of approximately identifying both the position and roughly the size of the damaged tissue, provided that the noise level is no larger than 3%. This is at least the case for synthetic observation data produced by the bidomain model and with zero geometrical uncertainties.

Example IV. In Examples I, II, III we used so-called iterative regularization. Many other techniques have been developed and it would be interesting to test various schemes on our problem. This is a delicate issue and deserves a thorough investigation. As a first step in this direction, we will now present a few experiments performed on coarser meshes – i.e. regularization by projection.

[2] One might increase the number of observations by measuring the body surface potential during several heart beats and/or by moving the electrodes at which the recordings are made.

[3] Recall that we performed 20 runs for each noise level.

Table 4
Results obtained with noisy observation data d_η, where $0 \leqslant \eta \leqslant 2\%$

Noise η (%)	Discrepancy		Manually	
	Error CM (%)	Error area (%)	Error CM (%)	Error area (%)
0.5	16.1	38.1	3.1	33.7
1.0	13.9	52.3	4.3	49.2
1.5	15.1	78.6	5.5	82.0
2.0	11.3	74.1	5.9	74.1

The table shows the *worst* results among the 20 experiments used to compute the averages presented in Table 3.

Table 5
Results obtained with noisy observation data d_η, where $3 \leqslant \eta \leqslant 5\%$

Noise η (%)	Error CM (%)	Error area (%)	Detection rate
3.0	7.8	46.0	19/20
4.0	4.9	59.0	14/20
5.0	8.4	61.0	10/20

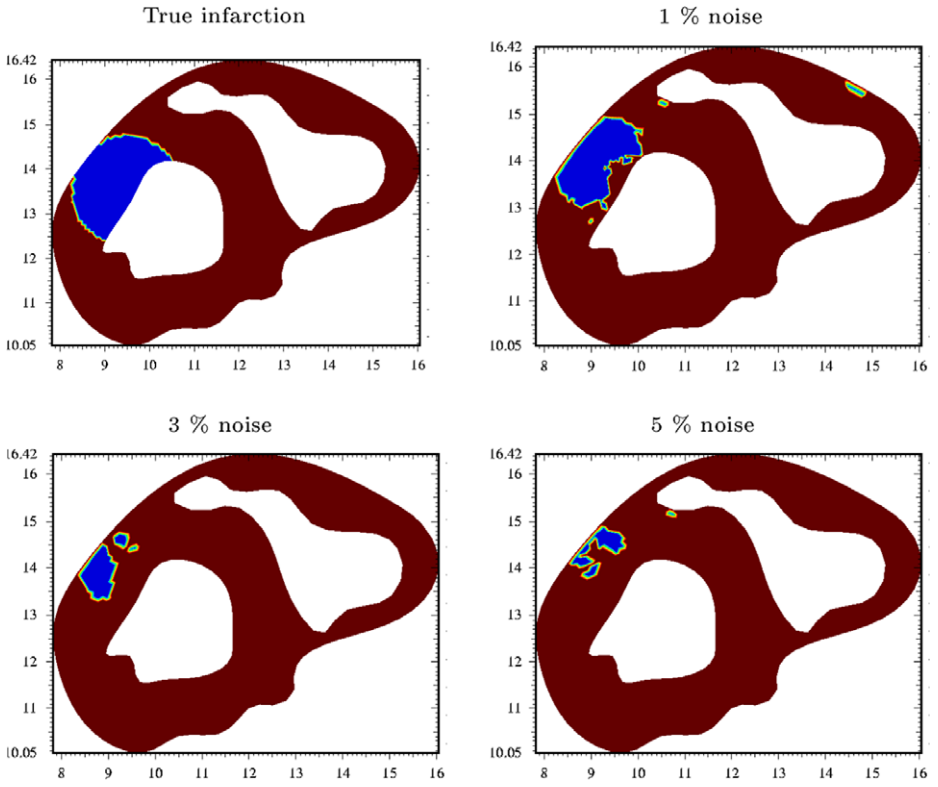

Fig. 6. The true ischemia and the estimates of it generated by Algorithm 3.1 with 1%, 3% and 5% Gaussian noise in the observation data.

In the experiments presented above, the level set function ϕ and the potential u were discretized in terms of the same mesh on the heart H (using 4059 nodes in H). It is of course possible to reduce the degrees of freedom for ϕ and thereby strengthen the projective regularization effect. Table 6 shows results obtained in this way. (The number of nodes reported in this table is the degrees of freedom used to discretize ϕ). These results indicate that additional regularization tools might improve the performance of our scheme. Not only is the accuracy in the estimates for the center of mass (CM) and the area of the ischemia better on coarser meshes, but the number of Landweber iterations needed is significantly reduced. These numbers were generated with

Table 6
Numerical results obtained with various degrees of freedom for the discrete level set function ϕ

# Nodes	Error in CM (%)	Error in area (%)	# Iterations
4059	0.7	16.2	43
1093	0.8	10.9	19
312	0.5	10.3	16

The forward problem for the potential u was solved on the fine grid used in Examples I, II, III.

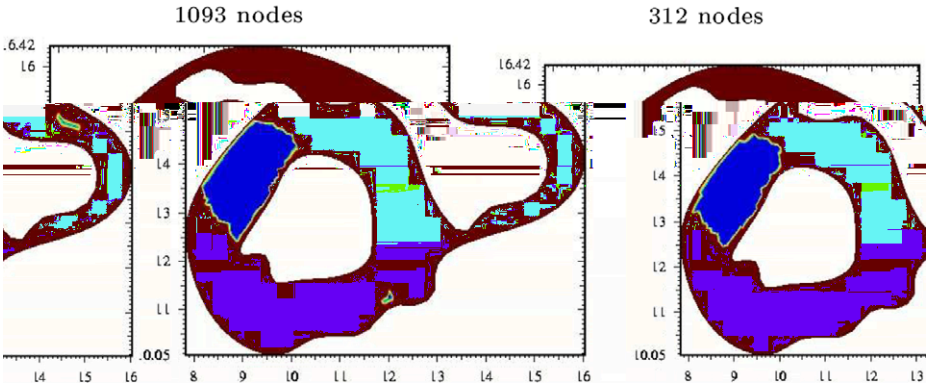

Fig. 7. The estimates generated with 1093 and 312 degrees of freedom for the level set function ϕ. These figures should be compared with the true infarction depicted in Fig. 4(a) and the result obtained with 4059 nodes shown in Fig. 4(d).

noise free observation data, and the iteration process was stopped manually at the minimum error in the CM. Qualitative information about the performance of our scheme on coarser meshes can be found in Fig. 7, which should be compared with Fig. 4(a) and (d) (Fig. 4(d) was generated with 4059 degrees of freedom for ϕ).

These experiments indicate rather strongly that the potential u and the level set function ϕ should be discretized on different meshes. However, involving several grid levels makes the programming more difficult, and the geometrical properties of the heart put restrictions on how coarse meshes that can be applied. The design of an "optimal" scheme for handling these issues is an open problem.

5. Summary and conclusions

We have introduced a mathematical framework and an algorithm suitable for identifying ischemic heart disease. Our approach is based on biological knowledge about the distribution of the transmembrane potential in the heart during rest, and modern mathematical methods for PDEs. More specifically, since the transmembrane potential is approximately piecewise constant during rest, taking one value in damaged tissue and a different one in the healthy region, it is possible to apply level set techniques to incorporate the effect of an ischemia on simulated ECG recordings.

Based on these observations, we formulated an inverse problem, with the level set function as the unknown, for identifying heart infarctions from ECG measurements. This lead to a minimization problem for a suitable cost-functional subject to a constraint expressed in terms of an elliptic PDE. To approximately solve this minimization problem, we applied the Landweber scheme. This method requires the partial derivatives of the cost-functional, which we computed with the adjoint problem approach. It is the use of the dual problem that makes our algorithm fast, and consequently might making it applicable in practical situations. In 2D our scheme requires 15–40 iterations and hence 2–3 min wall time on a standard laptop[4] running the Linux operating system.

Through a series of numerical experiments in 2D, using a heart in torso geometry with a realistic fiber structure, we illuminated both qualitative and quantitative properties of our algorithm. It turned out that the

[4] We performed our experiments on an IBM ThinkPad T40.

scheme was not very sensitive with respect to the smoothing parameter used in the level set framework. Moreover, for synthetic observation data generated by full bidomain simulations, we managed, provided that the noise level was less or equal to 3%, to roughly recover the position and size of the ischemia. However, whether this scheme is applicable in clinical situations is still unclear; 3D simulations, preferable with real world data, must be undertaken, and uncertainties regarding various geometrical aspects must be investigated.

Acknowledgement

We would like to thank the referee for several interesting and useful comments.

References

[1] G.W. Beeler, H. Reuter, Reconstruction of the action potential of ventricular myocardial fibres, J. Physiol. 268 (1977) 177–210.
[2] M. Burger, S. Osher, A survey on level set methods for inverse problems and optimal design, Eur. J. Appl. Math. 16 (2005) 263–301.
[3] E. Carmeliet, Cardiac ionic currents and acute ischemia: from channels to arrhythmias, Physiol. Rev. 79 (1999) 917–1017.
[4] A. Cimponeriu, C. Starmer, A. Bezerianos, A theoretical analysis of acute ischemia and infarction using ecg reconstruction on a 2-d model of myocardium, IEEE Trans. Biomed. Eng. 48 (1) (2001) 41–54.
[5] D. Colton, R. Kress, Inverse Acoustic and Electromagnetic Scattering Theory, second ed., Springer-Verlag, 1998.
[6] D. DiFrancesco, D. Noble, A model of cardiac electrical activity incorporating ionic pumps and concentration changes, Philos. Trans. R. Soc. Lond. Biol. 307 (1985) 353–398.
[7] O. Dössel, Inverse problem of electro- and magnetocardiography: review and recent progress, Int. J. Bioelectromagn. 2 (2000).
[8] H.W. Engl, M. Hanke, A. Neubauer, Regularization of Inverse Problems, Kluwer Academic Publishers, 1996.
[9] L.C. Evans, Partial Differential Equations, American Mathematics Society, 1998.
[10] K.R. Foster, H.P. Schwan, Dielectric properties of tissue and biological materials: a critical review, Crit. Rev. Biomed. Eng. 17 (1989) 25–104.
[11] A. Ghodrati, F. Calderero, D.H. Brooks, G. Tadmor, R. MacLeod, A level set algorithm for the inverse problem of electrocardiography, in: 38th Asilomar Conference on Signals, Systems and Computers, Monterrey, California, USA, 7–10 November 2 (2004) 1590–1594.
[12] R.M. Gulrajani, Forward and inverse problems of electrocardiography, IEEE Eng. Med. Biol. 17 (1998) 84–101.
[13] F. Hanser, M. Seger, B. Tilg, R. Modre, G. Fisher, B. Messnarz, F. Hintringer, T. Berger, F.X. Roithinger, Influence of ischemic and infarcted tissue on the surface potential, Comput. Cardiol. 30 (2003) 789–792.
[14] B. Hopenfeld, J. Stinstra, R. Macleod, A mechanism for st depression associated with contiguous subendocardial ischemia, J. Cardiovasc. Electrophysiol. 15 (2004).
[15] J. Keener, J. Sneyd, Mathematical Physiology, Springer-Verlag, 1998.
[16] D. Kilpatrick, S.J. Walker, A validation of derived epicardial potential distributions by prediction of the coronary artery involved in acute myocardial infarction in humans, Circulation 76 (1987) 1282–1289.
[17] D. Li, C.Y. Li, A.C. Yong, D. Kilpatrick, Source of electrocardiographic ST changes in subendocardial ischemia, Circ. Res. 82 (1998) 957–970.
[18] G.T. Lines, M.L. Buist, P. Grøttum, A.J. Pullan, J. Sundnes, A. Tveito, Mathematical models and numerical methods for the forward problem in cardiac electrophysiology, Comput. Visualiz. Sci. 5 (2003) 215–239.
[19] C.H. Luo, Y. Rudy, A model of the ventricular cardiac action potential: depolarisation, repolarisation, and their interaction, Circ. Res. 68 (1991) 1501–1526.
[20] C.H. Luo, Y. Rudy, A dynamic model of the cardiac ventricular action potential, Circ. Res. 74 (1994) 1071–1096.
[21] O.M. Lysaker, B.F. Nielsen, Towards a level set framework for infarction modeling: An inverse problem, Int. J. Numer. Anal. Modell. 3 (2006) 377–394.
[22] M.C. MacLachlan, B.F. Nielsen, O.M. Lysaker, A. Tveito, Computing the size and location of myocardial ischemia using measurements of st-segment shift, IEEE Trans. Biomed. Eng. 53 (6) (2006) 1024–1031.
[23] M.C. MacLachlan, J. Sundnes, G.T. Lines, Simulation of ST segment changes during subendocardial ischemia using a realistic 3D cardiac geometry, IEEE Trans. Biomed. Eng. 52 (2005) 799–807.
[24] R.S. MacLeod, D.H. Brooks, Recent progress in inverse problems in electrocardiology, IEEE Eng. Med. Biol. 17 (1998) 73–83.
[25] R.S. MacLeod, M. Gardner, R.M. Miller, B.M. Horacek, Application of an electrocardiographic inverse solution to localize ischemia during cooronary angioplasty, J. Cardiovasc. Electrophysiol. 6 (1995) 2–18.
[26] A. Michailova, A. McCulloch, Model study of ATP and ADP buffering, transport of Ca^{2+} and Mg^{2+}, and regulation of ion pumps in ventricular myocyte, Biophys. J. 81 (2001) 614–629.
[27] W.T. Miller, D.B. Geselowitz, Simulation studies of the electrocardiogram I. The normal heart, Circ. Res. 43 (1978) 301–315.
[28] S. Osher, R. Fedkiw, Level Set Methods and Dynamic Implicit Surfaces, Applied Mathematical Sciences, vol. 153, Springer, 2003.
[29] Y. Rudy, H.S. Oster, The electrocardiographic inverse problem, Crit. Rev. Biomed. Eng. 20 (1992) 25–45.
[30] F. Santosa, A level-set approach for inverse problems involving obstacles, ESAIM: Contr. Optim. Calculus Variat. 1 (1996) 17–33.
[31] D. Schwartzman, I. Chang, J. Michele, M. Mirotznik, K. Foster, Electrical impedance properties of normal and chronically infarcted left ventricular myocardium, J. Intervent. Cardiac Electrophysiol. 3 (1999) 213–224.

[32] R.M. Shaw, Y. Rudy, Electrophysiologic effects of acute myocardial ischemia: a theoretical study of altered cell excitability and action potential duration, Cardiovasc. Res. 35 (1997) 256–272.
[33] K. Skouibine, W. Krassowska, Increasing the computational efficiency of a bidomain model of defibrillation using a time-dependent activating function, Biomed. Eng. 28 (2000) 772–780.
[34] J. Sundnes, Modeling the electrophysiology of ischemic ventricular cells, Tech. Report, Simula Research Laboratory, 2004.
[35] J. Sundnes, G.T. Lines, X. Cai, B.F. Nielsen, K.A. Mardal, A. Tveito, Computing the Electrical Activity in the Heart, Springer-Verlag, 2006.
[36] J. Sundnes, B.F. Nielsen, K.A. Mardal, X. Cai, A. Tveito, On the computational complexity of the bidomain and the monodomain models of electrophysiology, Ann. Biomed. Eng., in press.
[37] L. Tung, A bi-domain model for describing ischemic myocardial D-C potentials, Ph.D. thesis, MIT, Cambridge, 1978.
[38] R.L. Winslow, J. Rice, S. Jafri, E. Marban, B. O'Rourke, Mechanisms of altered excitation-contraction coupling in canine tachycardia-induced heart failure, II. Model studies, Circ. Res. 84 (1999) 571–586.